

## Location of the Neutron Dripline at Fluorine and Neon

D. S. Ahn,<sup>1</sup> N. Fukuda,<sup>1</sup> H. Geissel,<sup>5</sup> N. Inabe,<sup>1</sup> N. Iwasa,<sup>4</sup> T. Kubo,<sup>1,\*</sup>† K. Kusaka,<sup>1</sup> D. J. Morrissey,<sup>6</sup> D. Murai,<sup>3</sup> T. Nakamura,<sup>2</sup> M. Ohtake,<sup>1</sup> H. Otsu,<sup>1</sup> H. Sato,<sup>1</sup> B. M. Sherrill,<sup>6</sup> Y. Shimizu,<sup>1</sup> H. Suzuki,<sup>1</sup> H. Takeda,<sup>1</sup> O. B. Tarasov,<sup>6</sup> H. Ueno,<sup>1</sup> Y. Yanagisawa,<sup>1</sup> and K. Yoshida<sup>1</sup>

<sup>1</sup>RIKEN Nishina Center for Accelerator-Based Science, RIKEN, 2-1 Hirosawa, Wako, Saitama 351-0198, Japan

<sup>2</sup>Department of Physics, Tokyo Institute of Technology, 2-12-1 O-Okayama, Meguro, Tokyo 152-8551, Japan

<sup>3</sup>Department of Physics, Rikkyo University, 3-34-1 Nishi-Ikebukuro, Toshima, Tokyo 171-8501, Japan

<sup>4</sup>Department of Physics, Tohoku University, 6-3, Aramaki Aza-Aoba, Aoba-ku, Sendai, Miyagi 980-8578, Japan

<sup>5</sup>GSI, Helmholtzzentrum für Schwerionenforschung GmbH, Planckstraße 1, 64291 Darmstadt, Germany

<sup>6</sup>National Superconducting Cyclotron Laboratory, Michigan State University, 640 South Shaw Lane, East Lansing, Michigan 48824, USA



(Received 28 March 2019; published 18 November 2019)

A search for the heaviest isotopes of fluorine, neon, and sodium was conducted by fragmentation of an intense  $^{48}\text{Ca}$  beam at 345 MeV/nucleon with a 20-mm-thick beryllium target and identification of isotopes in the large-acceptance separator BigRIPS at the RIKEN Radioactive Isotope Beam Factory. No events were observed for  $^{32,33}\text{F}$ ,  $^{35,36}\text{Ne}$ , and  $^{38}\text{Na}$  and only one event for  $^{39}\text{Na}$  after extensive running. Comparison with predicted yields excludes the existence of bound states of these unobserved isotopes with high confidence levels. The present work indicates that  $^{31}\text{F}$  and  $^{34}\text{Ne}$  are the heaviest bound isotopes of fluorine and neon, respectively. The neutron dripline has thus been experimentally confirmed up to neon for the first time since  $^{24}\text{O}$  was confirmed to be the dripline nucleus nearly 20 years ago. These data provide new keys to understanding the nuclear stability at extremely neutron-rich conditions.

DOI: 10.1103/PhysRevLett.123.212501

How many neutrons can be added to an element before it becomes unbound? This is one of the fundamental questions for nucleonic many-body systems bound by strong interactions. However, the location of the neutron dripline, defined as the neutron-rich limit of bound nuclei, has been a long-standing issue [1], and is only known at present up to oxygen (atomic number  $Z = 8$ ) [2–6]. No confirmed extensions of the dripline above  $Z = 8$  have been made for nearly 20 years. This is in sharp contrast to the proton dripline, which is known to much higher  $Z$  numbers [1] for a number of reasons, including that it is located closer to stability due to the Coulomb interaction.

The location of the neutron dripline places significant constraints on models of nucleon-nucleon interactions and many-body correlations at the limit of isospin due to its high sensitivity to the nuclear mass. The location of the neutron dripline also provides a rigorous test of nuclear mass formulas [7–10], microscopic mass predictions by large-scale shell models [11], nuclear density functional theories [12], and *ab initio* theories [13–15]. Nuclear masses under extreme neutron-rich conditions not only provide tests of nuclear structure near and beyond the dripline, but also put stringent constraints on the equation of state of neutron-rich nuclear matter, which is a key to understanding neutron stars and supernovae [9,16,17].

The so-called oxygen anomaly, illustrated in Fig. 1, demonstrates the difficulty in predicting the neutron

dripline and its sensitivity to details of nuclear structure. The sudden leap of the neutron dripline from carbon ( $^{22}\text{C}$ ), nitrogen ( $^{23}\text{N}$ ), oxygen ( $^{24}\text{O}$ ), all having neutron number  $N = 16$ , to fluorine ( $Z = 9$ ), where the heaviest known isotope is  $^{31}\text{F}$  with  $N = 22$  [5], is so far unique. Adding only one proton to oxygen induces an extra stability involving at least six more neutrons. For neon ( $Z = 10$ ), the heaviest known isotope is  $^{34}\text{Ne}$  with  $N = 24$  [18]. The oxygen anomaly has not been well understood. For example, the finite-range droplet macroscopic model FRDM [7] and the global mass model KTUY [8] incorrectly predict the neutron dripline at  $^{26}\text{O}$ , while the Hartree-Fock-Bogoliubov mass model HFB-24 [9,10] predicts it to

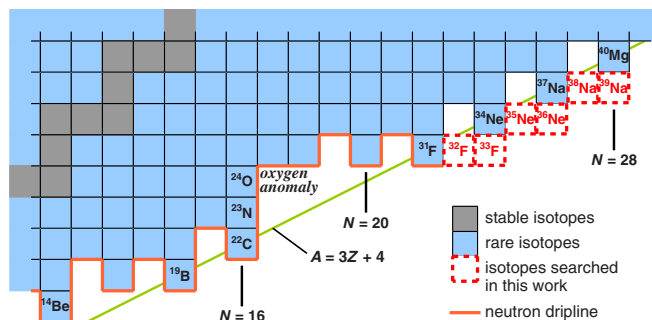


FIG. 1. Section of the nuclear chart showing the location of the isotopes studied in this work (red dotted squares).

be  $^{28}\text{O}$ . Recently, the mass of the resonance ground state of  $^{26}\text{O}$  has been found to be barely unbound by  $18 \pm 3(\text{stat}) \pm 4(\text{syst})$  keV with respect to the  $2n$  emission [19]. The instability of  $^{26-28}\text{O}$  has been attributed to a repulsive three-nucleon force [11], and is also indicated in *ab initio* calculations [13–15]. Other many-body correlations, such as the effects of dineutron correlation [20,21] and continuum coupling [22], may also play roles in the anomaly.

The extra stability of neutron-rich fluorine and neon relative to oxygen has also been attributed to the emergence of the island of inversion ( $Z = 10\text{--}12$ ,  $N = 20\text{--}22$ , and their neighbors), where the ground states gain energy by strong deformation due to spontaneous symmetry breaking [23–25]. An interesting suggestion has been made by Tanihata [26], where the neutron dripline is related to closing (sub)shell orbitals, as in  $^8\text{He}$  with  $N = 6$  that closes the  $1p_{3/2}$  orbital, and  $^{22}\text{C}$ ,  $^{23}\text{N}$ , and  $^{24}\text{O}$  with  $N = 16$  that closes the  $2s_{1/2}$  orbital. The suggestion is that a nucleus close to the neutron dripline has an increased binding at a closed shell and becomes unbound when one or even a pair of neutrons is added in a new orbital above a closed orbital. Adding one neutron makes the nucleus more unbound due to the loss of the pairing energy. If the fluorine and neon isotopes with  $N > 20$  have significant  $2p_{3/2}$  occupancy as in the neighboring  $p$ -wave halo nuclei such as  $^{31}\text{Ne}$  [27–29], the dripline at fluorine and neon may be due to closing the  $2p_{3/2}$  orbital, making the dripline nuclei  $^{33}\text{F}$  and  $^{34}\text{Ne}$  with  $N = 24$ .

This Letter presents new results for the neutron dripline for fluorine, neon, and sodium by searching for the new isotopes  $^{32,33}\text{F}$ ,  $^{35,36}\text{Ne}$ , and  $^{38,39}\text{Na}$ , as indicated in Fig. 1. The production of these isotopes was investigated at the Radioactive Isotope Beam Factory (RIBF) at RIKEN [30] by the fragmentation of a  $^{48}\text{Ca}$  beam at 345 MeV/nucleon with a 20-mm-thick beryllium target. We attempted to observe the isotopes beyond the mass number  $A = 3Z + 4$  line [5,18,31], where the most neutron-rich known isotopes are located. The typical beam intensity was as high as  $\sim 450$  particle nA ( $\sim 3 \times 10^{12}$  particles/s). The projectile fragments were separated and identified with the large-acceptance in-flight separator BigRIPS [32], which consists of two stages (see Fig. 1 of Ref. [33]): the first stage provides isotopic separation based on the magnetic rigidity analysis combined with the energy-loss analysis through a wedge-shaped achromatic degrader and the second stage provides particle identification as well as further separation using another wedge-shaped achromatic degrader. The degraders were placed at the momentum-dispersive intermediate foci in the two stages, while the isotope separation was accomplished using slits installed at achromatic foci at the end of each stage.

The search was conducted with two settings of the BigRIPS separator which we call the  $^{33}\text{F}$  setting and the  $^{36}\text{Ne} + ^{39}\text{Na}$  setting. In both settings, the magnetic rigidity

( $B\rho$ ) value was set to 9.385 Tm from the target to the first degrader to accept the momentum distributions of  $^{33}\text{F}$ ,  $^{36}\text{Ne}$ , and  $^{39}\text{Na}$  isotopes ( $^{36}\text{Ne}$  centered) due not only to their similar values of  $A/Z$ , but also due to the thick target with the large momentum acceptance of the separator. Neighboring isotopes including  $^{32}\text{F}$ ,  $^{35}\text{Ne}$ , and  $^{38}\text{Na}$  also had a reasonably large acceptance. In the  $^{33}\text{F}$  setting the  $B\rho$  value after the first degrader was tuned so as to transmit  $^{33}\text{F}$  (8.804 Tm), while in the  $^{36}\text{Ne} + ^{39}\text{Na}$  setting the  $B\rho$  value was tuned for the average of those for  $^{36}\text{Ne}$  and  $^{39}\text{Na}$  (8.721 Tm). In the latter setting, the  $^{36}\text{Ne}$  and  $^{39}\text{Na}$  fragments were peaked at approximately 7 mm on opposite sides of the center at the exit of the first stage. In addition, some  $^{32}\text{F}$ ,  $^{35,36}\text{Ne}$ , and  $^{37}\text{Na}$  ( $^{35}\text{Ne}$  and  $^{37,38}\text{Na}$ ) fragments had a high transmission in the  $^{33}\text{F}$  ( $^{36}\text{Ne} + ^{39}\text{Na}$ ) setting. For example,  $^{38}\text{Na}$  fragments nearly follow the central trajectory in the  $^{36}\text{Ne} + ^{39}\text{Na}$  setting. The fragment separator settings were based on detailed simulations using the LISE++ code [34].

The particle identification relied on the combination of energy loss ( $\Delta E$ ), time of flight (TOF), and  $B\rho$  measurements, from which  $Z$  and  $A/Z$  of fragments were deduced [35,36]. The TOF was measured over the 23-m flight path by two thin plastic scintillators with sizes of 240 mm (H)  $\times$  90 mm (V)  $\times$  3 mm (t) and 120 mm  $\times$  90 mm  $\times$  3 mm installed at the intermediate and final foci of the second stage, respectively. The  $\Delta E$  was measured with a four-element silicon detector stack with identical sizes of 50 mm  $\times$  50 mm  $\times$  0.45 mm installed at the final focus. The  $B\rho$  was determined from a position measurement at the intermediate focus based on the left-right time difference in the plastic scintillator. The rms position resolution was 3.7 mm that gave a corresponding  $B\rho$  resolution sufficient for the present mass region. A set of position-sensitive parallel plate avalanche counters [37] was installed at each of the first, intermediate, and final foci to verify the trajectories in the off-line analysis and to calibrate the position measurement with the scintillator. Background events, including those due to signal pileup, reactions in the detectors, and channeling in the silicon detectors, were rejected using the procedure described in Ref. [36].

The momentum acceptance of the separator was set to  $\pm 3\%$ . The slits at the final foci in the first and second stages were set to  $\pm 15$  and  $\pm 20$  mm, respectively. Achromatic aluminum degraders with mean thicknesses of 15 and 7 mm were used in the first and second stages, respectively. The two-stage separation, together with a 450-mm-thick horn-shaped iron collimator placed at the exit of the first stage, effectively reduced unwanted events including strong light-particle contaminants such as tritons. The remaining light particles were removed from the data stream by raising the trigger threshold.

Figures 2(a) and 2(b), respectively, show the  $Z$  vs  $A/Z$  particle identification spectra from the measurements with

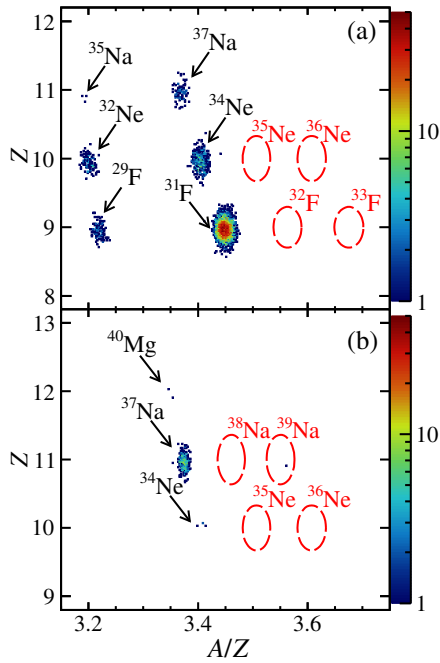


FIG. 2. Particle identification spectra as a function of  $Z$  and  $A/Z$  are shown for the settings tuned for (a)  $^{33}\text{F}$  and (b)  $^{36}\text{Ne} + ^{39}\text{Na}$ . See the text for details.

the  $^{33}\text{F}$  and  $^{36}\text{Ne} + ^{39}\text{Na}$  settings during which the beryllium target was irradiated with  $1.4 \times 10^{17}$  and  $7.8 \times 10^{16}$   $^{48}\text{Ca}$  ions in 14 and 7.8 h, respectively. In the  $^{33}\text{F}$  setting, no events were observed that would be consistent with  $^{32,33}\text{F}$  and  $^{35,36}\text{Ne}$ , while 3938 and 115 counts were observed for  $^{31}\text{F}$  and  $^{34}\text{Ne}$  (isotone of  $^{33}\text{F}$ ), respectively. In the  $^{36}\text{Ne} + ^{39}\text{Na}$  setting, no events were observed for  $^{35,36}\text{Ne}$  and  $^{38}\text{Na}$ , while 4 and 363 counts were observed for  $^{34}\text{Ne}$  and  $^{37}\text{Na}$  (isotone of  $^{36}\text{Ne}$ ), respectively. Furthermore, one count was observed for  $^{39}\text{Na}$ , while no counts for  $^{38}\text{Na}$ . These spectra demonstrate sufficient separation among different nuclides and excellent background rejection. The rms  $A/Z$  and  $Z$  resolutions were 0.24% and 1.1%, respectively.

The LISE++ simulations were confirmed by observation of strongly produced isotones that follow almost identical trajectories to the isotopes searched for. From the measurement with the parallel plate avalanche counters at the achromatic final focus in each stage,  $^{34}\text{Ne}$  and  $^{37}\text{Na}$ , the isotones of  $^{33}\text{F}$  and  $^{36}\text{Ne}$ , were found to follow the predicted trajectories in the  $^{33}\text{F}$  and  $^{36}\text{Ne} + ^{39}\text{Na}$  settings, respectively. The targeted isotopes would have had the predicted large acceptance, but since no events were observed for  $^{32,33}\text{F}$ ,  $^{35,36}\text{Ne}$ , and  $^{38}\text{Na}$ , these isotopes are either unbound or were produced at an extremely low rate.

To quantitatively assess the possibility that  $^{32,33}\text{F}$ ,  $^{35,36}\text{Ne}$ , and  $^{38}\text{Na}$  are bound but unobserved, systematic measurements of the production cross sections were performed as a function of mass number, in which the separator was

tuned for several different settings to cover  $^{23-27,29,31}\text{F}$ ,  $^{24-28,30,32,34}\text{Ne}$ , and  $^{35,37}\text{Na}$ . These data were compared to the well-known predictions from the EPAX 2.15 systematics [38] and the  $Q_g$  systematics [39,40]. These predictions are used to extrapolate the observed cross sections and estimate the expected yields for these unobserved isotopes and thus provide estimates of the confidence levels that these isotopes are particle unbound. The cross sections used the transmission values from the LISE++ code, where the momentum distribution assumed the parametrization at current energies which takes into consideration the low-momentum tail in the distribution [41,42]. The evaluation also included the transmission loss due to secondary reactions that occur in the materials along the path through the separator. The systematic uncertainty in overall normalization of the deduced cross sections was less than 30% and mainly due to the beam intensity normalization and transmission.

Figure 3 shows the measured cross sections along with the predictions. The EPAX 2.15 systematics are in good agreement with the data. The logarithmic slope as well as the absolute cross sections are fairly well reproduced. Note that the EPAX 2.15 was used because it has been found to reproduce cross sections in this mass region better than the EPAX 3.01 [42]. The  $Q_g$  systematics uses a fit of the measured cross sections  $\sigma(Z, A)$  on the neutron-rich side to the exponential function  $\sigma(Z, A) = f(Z) \exp(Q_g/T)$  that is extrapolated to the unobserved isotopes. Here,  $Q_g(Z, A)$ ,  $T$ , and  $f$  represent the difference of mass excesses between the projectile and the fragment, an effective temperature, and a normalization, respectively. The mass inputs for  $Q_g$  for the known bound isotopes are based on the AME2016 evaluation [43,44], while the unobserved ones such as  $^{33}\text{F}$  ( $^{32}\text{F}$ )

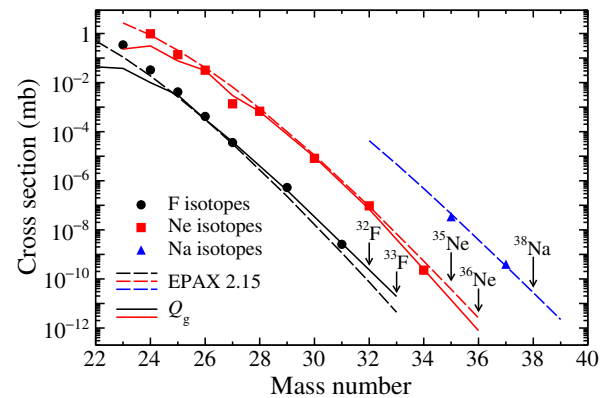


FIG. 3. Production cross sections measured for the fragmentation of  $^{48}\text{Ca}$  at 345 MeV/nucleon are shown for the neutron-rich fluorine (black solid circles) and neon (red solid squares) isotopes. Prediction from the EPAX 2.15 and  $Q_g$  systematics are shown for the fluorine (neon) isotopes by the black (red) dashed and solid curves, respectively. Those of  $^{35}\text{Na}$  and  $^{37}\text{Na}$  (blue solid triangles) are also shown along with the EPAX 2.15 predictions (blue dashed curve).

TABLE I. Production cross sections ( $\sigma$ ) of unobserved  $^{32,33}\text{F}$  and  $^{35,36}\text{Ne}$  estimated by the EPAX 2.15 and  $Q_g$  systematics and their expected yields obtained with the LISE++ simulations. Those of unobserved  $^{38}\text{Na}$ , based on the EPAX 2.15 systematics, are also listed. See text.

Isotope	Method	$\sigma$ (fb)	Expected yields <sup>d</sup>
$^{32}\text{F}^a$	EPAX	73.5	$323 \pm 97$
	$Q_g$	$258 \pm 76$	$(1.14 \pm 0.33) \times 10^3$
$^{33}\text{F}^a$	EPAX	4.39	$21.5 \pm 6.5$
	$Q_g$	$21.6 \pm 7.5$	$106 \pm 37$
$^{35}\text{Ne}^a$	EPAX	37.8	$177 \pm 53$
	$Q_g$	$14.8 \pm 3.6$	$69.1 \pm 16.7$
$^{36}\text{Ne}^b$	EPAX	2.58	$15.5 \pm 4.7$
	$Q_g$	$0.839 \pm 0.222$	$5.03 \pm 0.96$
$^{38}\text{Na}^c$	EPAX	27.4	$61.9 \pm 18.6$

<sup>a</sup> $^{33}\text{F}$  setting.

<sup>b</sup>Total of the  $^{33}\text{F}$  and  $^{36}\text{Ne} + ^{39}\text{Na}$  settings.

<sup>c</sup> $^{36}\text{Ne} + ^{39}\text{Na}$  setting.

<sup>d</sup>Errors shown for the EPAX 2.15 and  $Q_g$  systematics are due to the normalization uncertainty and the fitting error, respectively. See text.

assumed zero two-neutron (one-neutron) separation energy. The fitted  $T$  parameter obtained was 3.2 MeV (2.8 MeV) for fluorine (neon).

Table I summarizes the extrapolated cross sections and the expected yields estimated using the LISE++ code. We evaluated the confidence level, CL, from the probability that the isotope is not observed by chance (complementary event). The probability was calculated using its expected yield and the Poisson probability distribution, corresponding to  $1 - \text{CL}$ . For unobserved  $^{33}\text{F}$ , the EPAX 2.15 systematics predicts 22 counts, so that the probability can be calculated to be  $3 \times 10^{-10}$ . Thus,  $^{33}\text{F}$  is unbound (or the existence of bound  $^{33}\text{F}$  is excluded) at  $\text{CL} = 1 - 3 \times 10^{-10}$ .  $^{32}\text{F}$  is also unbound, as the expected yield is even larger. If the  $Q_g$  systematics is employed, these CL's are even closer to one due to larger expected yields. Therefore, the conclusion is that  $^{31}\text{F}$  is the dripline nucleus of fluorine. For unobserved  $^{36}\text{Ne}$ , the  $Q_g$  systematics predicts  $5.03 \pm 0.96$  counts for the total expected yields of the  $^{33}\text{F}$  setting (2.73 counts) and  $^{36}\text{Ne} + ^{39}\text{Na}$  setting (2.30 counts), giving  $99.3^{+0.4}_{-1.0}\%$  for the CL, where the uncertainties come from the fitting errors. Similarly to  $^{32}\text{F}$ , the CL for unobserved  $^{35}\text{Ne}$  is even larger. Thus the existence of bound  $^{35,36}\text{Ne}$  can also be excluded with high CL's. The EPAX 2.15 systematics predicts higher yields, giving even larger CL's. Again, these results provide evidence that  $^{34}\text{Ne}$  is the dripline nucleus of neon. For unobserved  $^{38}\text{Na}$ , the EPAX 2.15 systematics gives a high CL, excluding the existence of bound  $^{38}\text{Na}$ . The observation of one event for  $^{39}\text{Na}$  seems to suggest the existence of bound  $^{39}\text{Na}$ , but the present measurement with such low statistics does not permit a firm assignment of its particle stability. Thus, this study

extends the knowledge of the neutron dripline up to  $Z = 10$ .

The present dripline results can be compared with theoretical predictions. The FRDM mass formula in 2012 correctly predicts the position of the fluorine and neon driplines, while it predicts the previously observed  $^{31}\text{Ne}$  to be unbound with respect to the  $1n$  decay; however, it is only by 120 keV [7]. The KTUY mass formula incorrectly predicts the fluorine dripline to fall at  $^{29}\text{F}$ , while it correctly predicts the neon dripline as  $^{34}\text{Ne}$ , although the bound  $^{31}\text{Ne}$  is predicted to be unbound [8]. The HFB-24 calculation also fails near the fluorine dripline as it incorrectly predicts  $^{29}\text{F}$  and  $^{26}\text{F}$  as the dripline and unbound nuclei, respectively [9,10]. For neon, the HFB-24 does correctly predict the dripline, but yet it predicts the bound  $^{31}\text{Ne}$  as unbound. Thus, the current delineation of the dripline for fluorine and neon contrasts significantly with these models.

The simple picture proposed by Tanihata predicts that the isotopes with  $N = 24$  would be the last bound nuclei for fluorine and neon [26]. The present results support that Tanihata's suggestion is applicable to the dripline of neon but not the dripline of fluorine. Note, however, that the suggestion assumes a spherical shape with dominant  $2p_{3/2}$  occupancy of valence neutrons for  $N > 20$ , and the single particle state is fully degenerate with respect to angular momentum. As pointed out in Ref. [26], if a nucleus is deformed, the Nilsson model is applicable and single particle states with a given asymptotic quantum number have a degeneracy of two. Then, the end of the bound nuclei, as in the present case, would be  $N = 22$  for fluorine, thereby indicating deformed ground states of the neutron-rich fluorine isotopes. This would be indicative of extending the island of inversion down to the neutron dripline at fluorine, as is indicated in the recent in-beam  $\gamma$ -ray spectroscopy for  $^{29}\text{F}$  [45]. It is interesting to note that a recent large-scale shell model [46] predicts that  $^{31}\text{F}$  has a large mixture of intruder configurations, having characteristics of nuclei in the island of inversion. For neon, this shell model predicts a lower excitation energy for the first  $2^+$  state of  $^{34}\text{Ne}$  than  $^{32}\text{Ne}$  [47], indicating  $^{34}\text{Ne}$  is strongly deformed. The mixing of  $2p_{3/2}$  and  $1f_{7/2}$  single particle states of neutrons in  $^{34}\text{Ne}$  is expected from this calculation, also in line with the Nilsson picture. Currently, this shell model and *ab initio* calculations do not provide predictions on the location of the neutron dripline for  $Z > 8$ . Thus, the present results present a new challenge to these state-of-the-art theoretical calculations to predict the neutron dripline of fluorine and neon. The current results combined with such theories would shed light on the many-body correlations and nucleon-nucleon interactions at extreme neutron-rich conditions. Since  $^{31}\text{F}$  and  $^{34}\text{Ne}$  are probably very weakly bound, it would also be interesting to see if these nuclei have a halo structure similar to that found in neighboring  $^{31}\text{Ne}$  [27–29] and  $^{37}\text{Mg}$  [48,49].

In summary, we have investigated the production of  $^{32,33}\text{F}$ ,  $^{35,36}\text{Ne}$ , and  $^{38,39}\text{Na}$  using the fragmentation of an intense  $^{48}\text{Ca}$  beam on a thick beryllium target and the new-generation in-flight separator BigRIPS at RIKEN RIBF. We observed no events for  $^{32,33}\text{F}$ ,  $^{35,36}\text{Ne}$ , and  $^{38}\text{Na}$  and one event for  $^{39}\text{Na}$  from a substantial irradiation. The comparison of no events with the expected yields showed that existence of particle-bound states of these unobserved isotopes was excluded with high confidence levels. Thus, the conclusion is that the heaviest bound nuclei are  $^{31}\text{F}$  and  $^{34}\text{Ne}$  for fluorine and neon isotopes, respectively. The location of the neutron dripline has thus been extended (now up to  $Z = 10$ ) for the first time in nearly 20 years. The heaviest known isotopes for the next four elements are  $^{37}\text{Na}$  [18],  $^{40}\text{Mg}$ ,  $^{43}\text{Al}$  [31], and  $^{44}\text{Si}$  [39], respectively, but their positions relative to the dripline are unknown. Locating the neutron dripline continues to be an important challenge for new-generation facilities [50], and the neutron-dripline search will continue to play an important role in studies of the underlying nuclear structure at extremely neutron-rich conditions.

The present experiment was carried out at the RIBF operated by RIKEN Nishina Center, RIKEN and CNS, University of Tokyo. We would like to thank the RIBF accelerator crew for delivering the intense  $^{48}\text{Ca}$  beam. This work was supported in part by JSPS KAKENHI Grant No. 16H02179, and by MEXT KAKENHI Grants No. 24105005 and No. 18H05404, and by the U.S. National Science Foundation under Cooperative Agreement No. PHY-1565546 (MSU).

\*Corresponding author.

kubo@ribf.riken.jp

†Present address: Facility for Rare Isotope Beams, Michigan State University, 640 South Shaw Lane, East Lansing, Michigan 48824, USA.

- [1] M. Thoennessen, *Rep. Prog. Phys.* **76**, 056301 (2013).
- [2] D. Guillemaud-Mueller *et al.*, *Phys. Rev. C* **41**, 937 (1990).
- [3] M. Fauerbach, D. J. Morrissey, W. Benenson, B. A. Brown, M. Hellström, J. H. Kelley, R. A. Kryger, R. Pfaff, C. F. Powell, and B. M. Sherrill, *Phys. Rev. C* **53**, 647 (1996).
- [4] O. B. Tarasov *et al.*, *Phys. Lett. B* **409**, 64 (1997).
- [5] H. Sakurai *et al.*, *Phys. Lett. B* **448**, 180 (1999).
- [6] T. Nakamura, H. Sakurai, and H. Watanabe, *Prog. Part. Nucl. Phys.* **97**, 53 (2017).
- [7] P. Möller, W. D. Myers, H. Sagawa, and S. Yoshida, *Phys. Rev. Lett.* **108**, 052501 (2012).
- [8] H. Koura, T. Tachibana, M. Uno, and M. Yamada, *Prog. Theor. Phys.* **113**, 305 (2005).
- [9] S. Goriely, N. Chamel, and J. M. Pearson, *Phys. Rev. C* **88**, 024308 (2013); **88**, 061302(R) (2013).
- [10] S. Goriely, *Nucl. Phys.* **A933**, 68 (2015).
- [11] T. Otsuka, T. Suzuki, J. D. Holt, A. Schwenk, and Y. Akaishi, *Phys. Rev. Lett.* **105**, 032501 (2010).
- [12] J. Erler, N. Birge, M. Kortelainen, W. Nazarewicz, E. Olsen, A. M. Perhac, and M. Stoitsov, *Nature (London)* **486**, 509 (2012).
- [13] G. Hagen, M. Hjorth-Jensen, G. R. Jansen, R. Machleidt, and T. Papenbrock, *Phys. Rev. Lett.* **108**, 242501 (2012).
- [14] H. Hergert, S. Binder, A. Calci, J. Langhammer, and R. Roth, *Phys. Rev. Lett.* **110**, 242501 (2013).
- [15] S. K. Bogner, H. Hergert, J. D. Holt, A. Schwenk, S. Binder, A. Calci, J. Langhammer, and R. Roth, *Phys. Rev. Lett.* **113**, 142501 (2014).
- [16] J. M. Lattimer and M. Prakash, *Phys. Rep.* **442**, 109 (2007).
- [17] K. Hebeler, J. M. Lattimer, C. J. Pethick, and A. Schwenk, *Astrophys. J.* **773**, 11 (2013).
- [18] M. Notani *et al.*, *Phys. Lett. B* **542**, 49 (2002).
- [19] Y. Kondo *et al.*, *Phys. Rev. Lett.* **116**, 102503 (2016).
- [20] L. V. Grigorenko, I. G. Mukha, and M. V. Zhukov, *Phys. Rev. Lett.* **111**, 042501 (2013).
- [21] K. Hagino and H. Sagawa, *Phys. Rev. C* **89**, 014331 (2014).
- [22] A. Volya and V. Zelevinsky, *Phys. At. Nucl.* **77**, 969 (2014).
- [23] E. K. Warburton, J. A. Becker, and B. A. Brown, *Phys. Rev. C* **41**, 1147 (1990).
- [24] T. Motobayashi *et al.*, *Phys. Lett. B* **346**, 9 (1995).
- [25] T. Motobayashi and H. Sakurai, *Prog. Theor. Exp. Phys.* **2012**, 03C001 (2012), and references therein.
- [26] I. Tanihata, D. Hirata, and H. Toki, *Nucl. Phys.* **A583**, 769 (1995).
- [27] T. Nakamura *et al.*, *Phys. Rev. Lett.* **103**, 262501 (2009).
- [28] M. Takechi *et al.*, *Phys. Lett. B* **707**, 357 (2012).
- [29] T. Nakamura *et al.*, *Phys. Rev. Lett.* **112**, 142501 (2014).
- [30] Y. Yano, *Nucl. Instrum. Methods Phys. Res., Sect. B* **261**, 1009 (2007).
- [31] T. Baumann *et al.*, *Nature (London)* **449**, 1022 (2007).
- [32] T. Kubo, *Nucl. Instrum. Methods Phys. Res., Sect. B* **204**, 97 (2003).
- [33] T. Ohnishi *et al.*, *J. Phys. Soc. Jpn.* **77**, 083201 (2008).
- [34] O. B. Tarasov and D. Bazin, *Nucl. Instrum. Methods Phys. Res., Sect. B* **266**, 4657 (2008), <http://lise.nsl.msui.edu/>.
- [35] T. Ohnishi *et al.*, *J. Phys. Soc. Jpn.* **79**, 073201 (2010).
- [36] N. Fukuda, T. Kubo, T. Ohnishi, N. Inabe, H. Takeda, D. Kameda, and H. Suzuki, *Nucl. Instrum. Methods Phys. Res., Sect. B* **317**, 323 (2013).
- [37] H. Kumagai, T. Ohnishi, N. Fukuda, H. Takeda, D. Kameda, N. Inabe, K. Yoshida, and T. Kubo, *Nucl. Instrum. Methods Phys. Res., Sect. B* **317**, 717 (2013).
- [38] K. Sümmerer and B. Blank, *Phys. Rev. C* **61**, 034607 (2000).
- [39] O. B. Tarasov *et al.*, *Phys. Rev. C* **75**, 064613 (2007).
- [40] O. B. Tarasov *et al.*, *Phys. Rev. Lett.* **102**, 142501 (2009).
- [41] O. Tarasov, *Nucl. Phys.* **A734**, 536 (2004).
- [42] H. Suzuki *et al.*, *Nucl. Instrum. Methods Phys. Res., Sect. B* **317**, 756 (2013).
- [43] W. J. Huang, G. Audi, M. Wang, F. G. Kondev, S. Naimi, and X. Xu, *Chin. Phys. C* **41**, 030002 (2017).
- [44] M. Wang, G. Audi, F. G. Kondev, W. J. Huang, S. Naimi, and X. Xu, *Chin. Phys. C* **41**, 030003 (2017).

- [45] P. Doornenbal *et al.*, *Phys. Rev. C* **95**, 041301(R) (2017).  
[46] E. Caurier, F. Nowacki, and A. Poves, *Phys. Rev. C* **90**, 014302 (2014).  
[47] P. Doornenbal *et al.*, *Phys. Rev. Lett.* **103**, 032501 (2009).  
[48] N. Kobayashi *et al.*, *Phys. Rev. Lett.* **112**, 242501 (2014).  
[49] M. Takechi *et al.*, *Phys. Rev. C* **90**, 061305(R) (2014).  
[50] T. Kubo, *Nucl. Instrum. Methods Phys. Res., Sect. B* **376**, 102 (2016).